Smart Agricultural Technology 2 (2022) 100029

Contents lists available at ScienceDirect

Smart Agricultural Technology

journal homepage: www.elsevier.com/locate/atech

Using UAV-based thermal imagery to detect crop water status variability in cotton

Lorena N. Lacerda[a,*], John L. Snider[a], Yafit Cohen[b], Vasileios Liakos[c], Stefano Gobbo[d], George Vellidis[a]

[a] Department of Crop and Soil Sciences, University of Georgia, 2360 Rainwater Road, Tifton, GA, 31793, USA
[b] Institute of Agricultural Engineering, Agricultural Research Organization (ARO), Volcani Center, Rishon LeZion 7505101, Israel
[c] Department of Agronomy and Agrotechnology, University of Thessaly, 41500 Larissa, Greece
[d] Department of Agronomy, Food, Natural Resources, Animals and the Environment (DAFNAE), University of Padova, Agripolis, Viale dell'Universita 16, 35020 Legnaro (Pd), Italy

ARTICLE INFO

Keywords:
Canopy temperature
Thermal images
Leaf water potential
Crop water stress index
Cotton
UAV

ABSTRACT

Plant-based measurements such as leaf water potential (LWP) are widely used for irrigation scheduling because they are accurate at indicating when irrigation is needed. Despite being a good indicator, scheduling irrigation with LWP is time consuming and scale-limited. The work reported in this study explored the potential of using thermal remote sensing to estimate cotton crop water status in the humid southeastern U.S.A. The study was conducted over two growing seasons (2018 and 2020) in southwestern Georgia, U.S.A using a complete randomized block design plot scheme with three irrigation treatments (0% ET_c (crop evapotranspiration; rainfed), 100% ET_c (well-irrigated), and 125% ET_c (over-irrigated). To monitor the irrigation treatment effects on cotton physiological responses, predawn LWP (LWP_{PD}), stomatal conductance (g_s) and leaf area index (LAI) data were collected in both growing seasons. UAV-based images collected in the thermal infrared waveband were used to calculate crop water stress index (CWSI) based on three different methodologies and evaluated as predictors of LWP_{PD}. Results in this study suggest that LWP_{PD} values above -0.45 MPa indicate a non-stressed crop. No negative effects in leaf stomatal conductance and crop growth were observed in 2018. In 2020, the less and more irregular precipitation led to significant differences in LAI and g_s, as well as in LWP_{PD}. A moderate to strong relationship was observed for all dates in 2020, with the CWSI based on the Monteith approach ($CWSI_{Monteith}$) showing the two highest R^2 values among the 3 dates (0.65 and 0.58) with low RMSE values of 0.02 and 0.04 MPa, respectively. Overall, the results showed that there is potential of using an affordable UAV-based thermal system to produce predicted LWP maps that are representative of the current field water status.

1. Introduction

Cotton (*Gossypium hirsutum* L.) is the most important fiber crop in the international commodity markets. It is also an extremely economically important crop in the U.S.A [1]. In 2021, approximately 4.5 million hectares were planted to cotton in the U.S.A with an average lint yield of 976 kg/ha mainly concentrated in the country's southern region [2]. From a global perspective, cotton production is mostly concentrated in semi-arid and arid regions often under irrigated conditions due to its negative response to excessive rainfall in certain developmental stages [3][4], as well as its requirements for high solar radiation levels and temperatures [5]. Even though its production is concentrated in arid areas, it can be cultivated under a variety of different water regimes [6][7].

In the state of Georgia, the average rainfall during the cotton growing season is sufficient to meet the crop water needs. Average precipitation between the months of April and October for the past 30 years is approximately 740 mm [8], whilst cotton requirements to achieve high yields in the same region are around 457 mm [9]. However, the distribution of rainfall during the growing season may not always align with the peak crop water requirements. An agronomic drought episode, even if short, at a critical stage of crop development can reduce the number

Abbreviations: $CWSI_{Jones1}$, Jones 1 crop water stress index; $CWSI_{Jones2}$, Jones 2 crop water stress index; $CWSI_{Monteith}$, Monteith crop water stress index; DAP, days after planting; ET_c, crop evapotranspiration; ET_0, reference evapotranspiration; g_s, stomatal conductance; K_c, crop coefficient; LAI, leaf area index; LWP_{PD}, predawn leaf water potential; PAR, photosynthetically active radiation; PGR, plant growth regulator; T_c, canopy temperature; T_{cr}, temperature of canopy-related pixels in a thermal images; T_{wet}, temperature of wet baseline; T_{dry}, temperature of dry baseline; UAV, unmanned aerial vehicle; VPD, vapor pressure deficit.

* Corresponding author.
E-mail address: lacerdalorena31@gmail.com (L.N. Lacerda).

https://doi.org/10.1016/j.atech.2021.100029
Received 1 November 2021; Received in revised form 20 November 2021; Accepted 20 November 2021

of floral buds, boll retention [7], boll weight and distribution [10] and final yield [11]. In addition, drought stress can cause reductions in photosynthetic rate caused by, among other factors, reductions in stomatal conductance [12]. As a result, approximately 50% of the cotton grown in Georgia is irrigated. Overirrigation can also be a problem since it can result in low irrigation efficiency by creating drainage problems in the soil and resulting in depressed yields [13]. In addition, excessive irrigation can negatively impact water resources, causing in some cases, the depletion of surface and ground water [14][15].

Because of the yield limitations imposed by water stress, a variety of irrigation scheduling techniques have been developed with the aim of improving the timing and amount of irrigation water applied and increasing irrigation water use efficiency [16][17][18]. Jones [19] divided the most commonly used irrigation scheduling methods into three main classes; 1) soil water measurement that includes irrigation based on soil water potential and soil water content, 2) soil water balance calculations, which involves estimating rainfall and evapotranspiration (ET), and 3) plant stress sensing, which is subdivided into tissue water status measurements and physiological responses. One direct plant stress indicator is leaf water potential (LWP).

Plant-based measurements such as LWP are widely used for irrigation scheduling [20][21][22] because of their accurate indication of when irrigation is needed. Although there has been some controversy around the effectiveness of LWP as an irrigation indicator due to temporal fluctuations caused by environmental conditions [19], authors have found satisfactory results for different crops [23][24]. In cotton, Argyrokastritis et al. [25] measured LWP under two different irrigation methods (full and deficit irrigation) and found that LWP for stressed plants was significantly lower than for the fully irrigated plants, which provides a key insight into the crop's water status and the need for irrigation. In a study conducted in 2016, predawn LWP thresholds were used for triggering irrigation resulting in a 7 to 31% increase in water use efficiency while achieving similar yields as a checkbook method (weekly irrigation based on crop phenological stages) commonly used by farmers [22].

Despite being a good indicator for irrigation scheduling, LWP measured with a Scholander pressure chamber is time consuming and scale limited [26][27] as each measurement in the field requires several minutes to perform with cumbersome equipment. In this context, authors have explored the use of remote sensing to detect or estimate crop water status as an alternative [28][29][30]. One approach is to calculate crop water stress index (CWSI) from thermal infrared image-based canopy temperature and to establish a relationship between CWSI and LWP [31]. LWP predicted from this relationship has shown high agreement with measured LWP in arid environments and has been used to map LWP variability [30].

In humid regions, the use of thermal infrared images to measure canopy temperature can be challenging when compared to arid regions [32]. Crops that exhibit isohydric behavior tend to show an increase in leaf temperature when experiencing water stress because of reduced transpiration as a result of stomatal closure [33]. However, leaf temperature is also highly dependent on other environmental factors such as relative humidity, air temperature, wind speed and incident radiation [34]. In humid environments, the lower vapor pressure deficit (VPD) results in smaller differences in canopy temperature between stressed and non-stressed plants since the air tends to be more saturated [33]. Moreover, the partial cloud cover which is commonly observed in humid climates causes rapid changes in canopy temperature within portions of a field making it difficult to capture whole-field images under uniform light conditions [35].

The overall goal of this study was to explore the potential of using an affordable UAV-based thermal imagery system to detect crop water stress in cotton in the humid environment of southern Georgia where relative humidity exceeds 80% for the majority of the growing season. Specific objectives were 1) to use UAV-based thermal images to predict LWP_{PD}, 2) to compare the relationship between CWSI derived from three different methodologies and 3) and to demonstrate the application of the CWSI/LWP relationship in creating representative predicted LWP_{PD} maps.

2. Materials and methods

2.1. Study site and management practices

A two-year study was conducted in 2018 and 2020 in two different experimental fields at the University of Georgia's Stripling Irrigation Research Park (SIRP) in Camilla, GA (Fig. 1). In 2018, 54 plots were established in a field of approximately 1 ha in size (31°16′43.33"N, 84°17′48.17"W). Plots consisted of 4 rows each with 12.2 m in length. The center 2 rows of each plot were used for data collection. Three different cultivars were planted at 2.5 cm depth on May 2nd. The three cultivars used were PHY 330 and PHY 490 (PhytoGen, Dow AgroSciences LLC, IN), and ST 6182 (GLT – Bayer Stoneville). Irrigation treatments consisted of 0% ET_c (crop evapotranspiration, 100% ET_c and 125% ET_c. A randomized complete block design was used with six replicates of each treatment (3 varieties × 3 irrigation treatments × 6 replicates).

In 2020, 27 plots were established in an experimental field with approximately 3.6 ha in size (31°16′58.88"N, 84°17′47.95"W). Plots had the same length and width as plots in 2018. The field was planted on May 13th with the DP 1646 (Deltapine, Bayer) cultivar. Irrigation treatments were the same as in 2018 and were combined with three plant growth regulator treatments (PGR). PGR treatments consisted of a control (no PGR application) a moderate (355 ml pix + 473 ml pix at first flower + 2 weeks) and aggressive treatment (296 ml at 8 leaf, 355 and 473 ml at first flower + 2 weeks). A randomized complete block design was used with three replicates of each treatment (3 irrigation treatments × 3 PGR treatments × 3 replicates).

2.2. Irrigation treatments

The irrigation treatments were applied using a linear move system with overhead sprinkler irrigation in 2018, and from three center pivot systems in 2020, both equipped with variable rate irrigation (VRI) technology. ET_c was estimated using the SmartIrrigation Cotton App [15]. In the SmartIrrigation App, ET_c is estimated daily from reference ET (ET_0) using meteorological data from the Camilla weather station (University of Georgia Weather Station Network) located within 300 m of both fields and a crop coefficient (K_c) extracted from a K_c curve that was validated for more than five years at SIRP [15]. Daily K_c was multiplied by daily ET_0 to estimate daily ET_c. The 100% ET_c treatment was based on the deficit between daily ET_c and rainfall and was considered a well-watered treatment. The 125% ET_c treatment irrigation amount was estimated by multiplying daily ET_c – precipitation by 1.25. This was considered an over-irrigated treatment. The rainfed treatment received irrigation until the squaring stage to help with initial development and growth. No supplemental water was applied for the remaining of the season. The irrigation amount per irrigation event was 19.05 mm in 2018 and 20.3 mm in 2020. The amounts were estimated to avoid runoff and were also based on the irrigation system capacity.

2.3. Field data collection

To monitor the irrigation treatment effects on cotton growth and physiological response, LWP_{PD}, leaf area index (LAI) and stomatal conductance (g_s) were collected in both seasons. Data collection was performed from squaring stage until the last week of irrigation. Measurements were collected weekly in 2018 and reduced to two-week intervals in 2020 due to personnel limitation. Predawn LWP was collected from 04:00 to 06:00 h for the uppermost fully expanded leaf of two plants in each plot using a Scholander pressure chamber (Model 615; PMS Instruments, Albany, OR). Cotton leaves were cut at the base of the petiole and sealed inside the chamber, where pressure was applied until

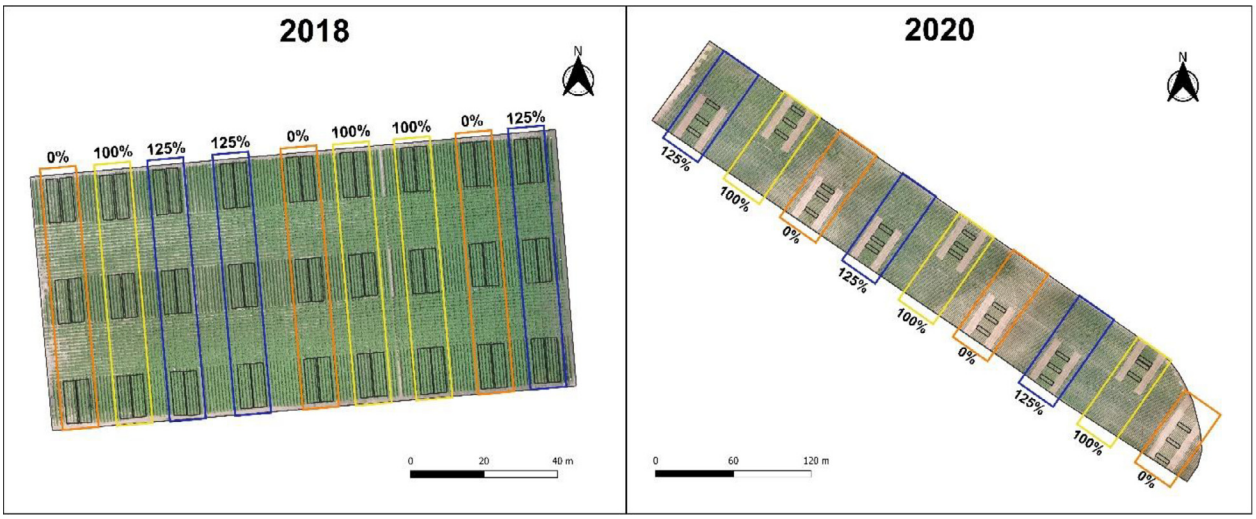

Fig. 1. Layout of fields in 2018 and 2020. Irrigation treatments are shown in different colors. Well-watered treatment is represented as 100% ET_c, and over-irrigated is represented as 125% Et_c.

xylem sap exuded from the petiole's cut surface. In-field LAI was collected using an AccuPAR LP-80 (Decagon Devices Inc., Pullman, WA) ceptometer. This equipment consists of two light probes connected to a datalogger. A small quantum sensor is placed on a tripod to collect above canopy photosynthetically active radiation (PAR) while an elongated probe containing multiple quantum sensors is placed under the canopy to collect below-canopy PAR values simultaneously. Two above and below measurements were taken in each plot with one measurement being taken with the long probe positioned parallel to the cotton rows, and one perpendicular to the rows. In addition, gas exchange measurements were taken from the uppermost fully expanded leaf in two plants in each plot. Gas exchange measurements were conducted from 12:00 to 14:00 h using an LI-6800 (LI-COR Biosciences, Lincoln, NE) portable photosynthesis system. The leaf chamber settings included a reference CO_2 concentration of 400 μmol mol^{-1}, a flow rate of 600 μmol s^{-1}, chamber light intensity = 1500 μmol m^{-2} s^{-1} photosynthetic active radiation (PAR), relative humidity = 60%, and air temperature = ambient temperature. Among the parameters measured, g_s was selected for analysis in this study.

2.4. UAV sensors and data acquisition

Remotely sensed data were collected using a 3DR Solo quadcopter (3D Robotics, Berkeley, CA, United States) equipped with a FLIR Vue Pro R (Model 640, 69°FOV, 9mm, 30Hz; FLIR Systems, Inc., Wilsonville, OR) camera. The camera was adapted to the UAV using a fixed mount and a GPS geotagger (sUAS LLC, Beltsville, MD) to geotag images during the flight. The FLIR Vue pro R uses an uncooled Vox microbolometer detector and collects 14-bit images (with embedded calibrated temperature values) in the 7.5 to 13.5 μm region of the electromagnetic spectrum.

Flights to collect thermal images began 65 days after planting (DAP) to ensure higher canopy coverage to mitigate the influence of background soil temperature on the imagery. Before each flight the camera was turned on for a period of 15 to 20 minutes to warm up. Flights were performed within 2 hours of solar noon on all dates between 12:00 and 14:00 h. In 2018, flights were performed at 50 m altitude at a speed of 4 m/s and 80% frontal and side overlap. The spatial resolution of the thermal images was 10.5 cm. In 2020, side and front overlaps for flights were the same as in 2018, but flights were performed at a higher altitude of 90 m and higher speed of 9 m/s due to the bigger experimental area used in that year. The spatial resolution in 2020 was 16.5 cm.

2.5. Image processing

UAV flight images were stitched using Pix4Dmapper software (Pix4D SA, Lausanne, Switzerland). The processing template was personalized to ensure the highest stitching quality. Ground control points (GCPs) were placed in the four corners of the field and used during the stitching process to increase projection accuracy. The position of each GCP was taken with a GPS receiver in the field and coordinates were then uploaded to Pix4Dmapper. GCPs were selected in at least 10 images for calibration.

Final thermal reflectance maps generated on Pix4Dmapper were then analyzed using ArcMap (ESRI, Redlands, CA, U.S.A) for data processing and extraction. Shapefile with plot boundaries were created based on the images from the first flight, that also served as a base for georeferencing for subsequent images throughout the season to further minimize discrepancies in the rows' locations between dates. In addition, a buffer area of 0.5 m was created between plot boundaries. Both measures were taken to avoid extraction of pixels from rows outside the plot area.

Canopy temperature extraction was performed using an empirical methodology demonstrated by Meron et al. [36]. This methodology is based on the assumptions 1) that canopy and soil-related pixels in thermal images are separated by upper and lower thresholds related to the air temperature as shown in Eq.1:

$$(T_{air} - 10) < T_{cr} < (T_{air} + 7) \quad (1)$$

where T_{air} is air temperature (°C) and T_{cr} is the temperature of canopy-related pixels in a thermal image, and 2) that canopy temperature is represented by an average temperature of the coolest 33% canopy-related pixels. In this step, mixed reflectance pixels commonly seen at the edges of rows are eliminated. The final canopy temperature is calculated using the class conditional histogram following Eq. 2.

$$T_c = \frac{\sum_{i=1}^{0.33n} T_{cr} * f_i}{\sum_{i=1}^{0.33n} f_i} \quad (2)$$

where T_c (°C) is the canopy temperature, f_i is the number of pixels in each class *cr* of the histogram, and *n* is the number of pixels retained after the non-crop related pixels were excluded.

2.6. Thermal camera accuracy

To assess the accuracy of the temperature measured by the FLIR Vue Pro R camera system, a low-cost reference surface (RS) structure was constructed to emulate the emissivity of a black body (Fig. 2). Black

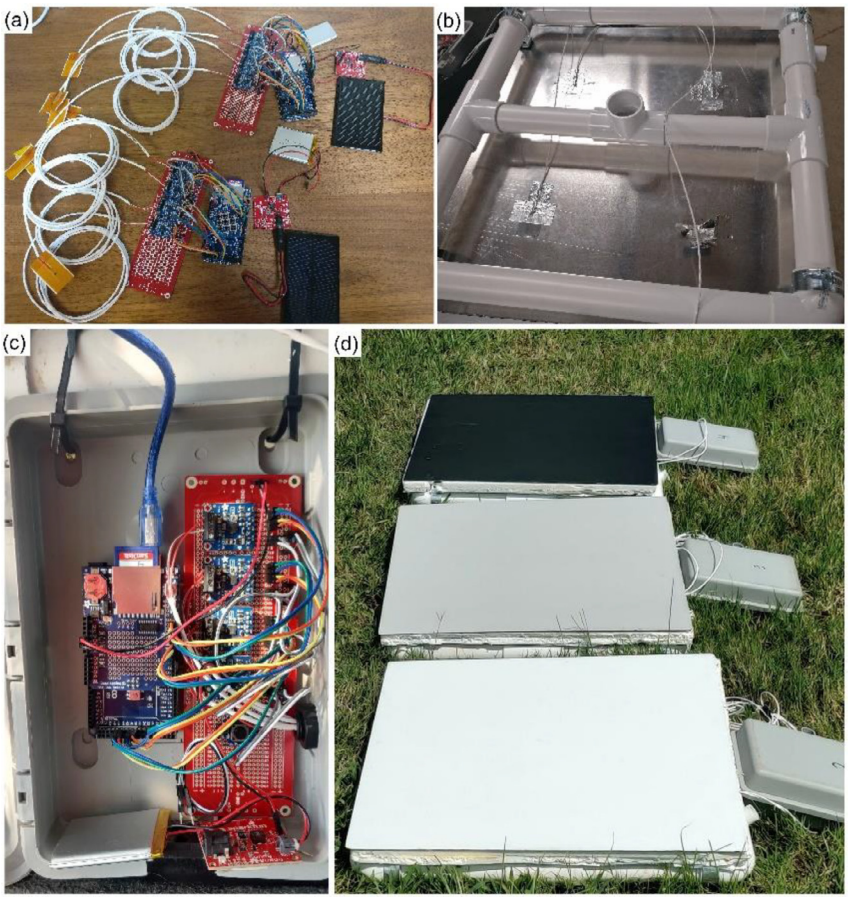

Fig. 2. Electronics for temperature sensing in real time (a), placement of RTDs in the aluminum plate (b), electrical junction box with boards (c), and white, gray, and black RS in the field (d).

bodies have emissivity of 1 and are regarded as perfect emitters. The emissivity of an object is defined as the ratio of energy radiated compared to that radiated from a black body [37]. The RS consisted of a 60 × 60 cm aluminum plate that was 2.2 cm thick. The size of the surfaces ensured that they would be represented by multiple pixels in the thermal images. One side of the plate was painted with a matte paint with high emissivity. To measure the surface temperature, four thin film platinum resistance temperature detectors (RTDs) with three conductors were attached to the bottom side of the plates. These sensors are classified as type A with an accuracy of +/- 0.15˚C. To enable real time temperature readings, an Arduino Mega embedded system (Arduino LLC, Torino, Italy) powered by rechargeable lithium batteries was used (Fig. 2a). The Arduino was programmed to take readings every 5 seconds. An RTD sensor amplifier with MAX31865 breakout (Adafruit Industries, NY, U.S.A) was used to connect the RTD sensors to the Arduino board and to ensure accuracy. The four sensors were attached to the bottom of the plate and covered by a 25 mm layer of expanded polystyrene insulation foam (Fig. 2b) to mitigate the effects of air temperature on the temperature readings and to avoid high temperature fluctuation in the plates. All electronics components were stored in a plastic project box to protect the boards from direct sunlight and dust (Fig. 2c). A frame constructed from plastic pipe was used to secure all structural components (plate, insulation foam and project box) together. During each flight, the surfaces were placed in the field at a central location to secure that the plates would appear in a high number of images during the flight (Fig. 2b,d).

In 2018, three surfaces painted black were placed in the field during the thermal flights to assess accuracy of temperature data extracted from the images. To obtain a wider range of known temperatures, two surfaces were modified and painted white and gray in 2020 (Fig. 2c). Average temperatures measured by the four RTD sensors were calculated for comparison with the thermal camera. The ThermaCAM Researcher Pro 2.10 software (FLIR Systems, Inc., Wilsonville, OR) was used for individual image analysis. For each flight, at least two images in which a RS appeared perpendicular to the camera were analyzed and the pixel temperature was extracted for comparison with averaged temperature measured from the four RTD sensors. Time stamps were used to ensure temperature values from both platforms were from the same period. The sensor temperature was plotted versus the temperature measured from the FLIR camera and good agreement between the two was observed (Fig. 3). An error of +1.54˚C was seen in 2018, and +2.18˚C in 2020, indicating that the image temperatures tended to be overestimated. However, error values were below the +/- 5˚C accuracy range expected for this type of sensor.

2.7. Crop water stress index

Canopy temperature data collected with the UAV-based thermal camera were used to calculate CWSI based on the following equation $CWSI = (T_c - T_{wet}) / (T_{dry} - T_{wet})$, where CWSI varies from 0 to 1, representing a crop without any water limitation and a non-transpiring crop, respectively [38], T_{wet} is the temperature of a fully transpiring leaf and T_{dry} is the temperature of a non-transpiring leaf. The wet and dry baselines were calculated using three different methodologies. The first CWSI ($CWSI_{Jones1}$) was calculated using theoretical dry and wet baselines based on the energy balance equation suggested by Jones [39]. The second CWSI ($CWSI_{Jones2}$) used the same theoretical wet baseline, but the dry baseline was calculated empirically by adding 5˚C to the air temperature. The third CWSI ($CWSI_{Monteith}$) was calculated using a theoretical wet baseline based on Monteith and Unsworth [40] and the same empirical dry baseline used on $CWSI_{Jones2}$. Meteorological data used for baseline calculations was collected from the Camilla weather station.

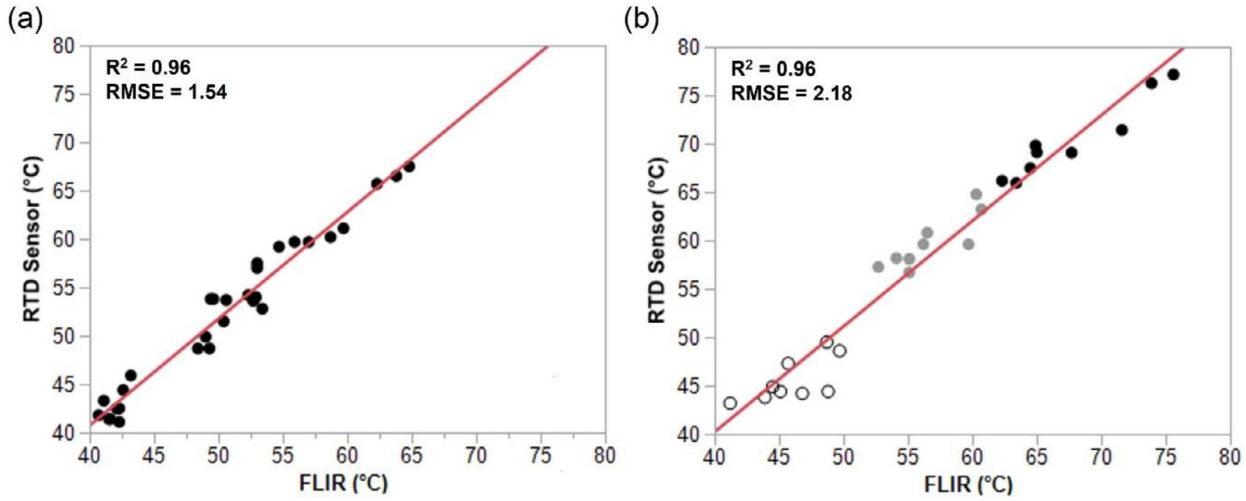

Fig. 3. Comparison between FLIR-based temperature and RTD sensor temperature in (a) 2018, and (b) 2020. White, grey, and black points in 2020 refer to the different colored surfaces.

Data recorded every 15 minutes from 12:00 to 14:00 h were averaged and used in calculations. The average of the 33% coolest pixels of each plot was used as T_c in the CWSI equation.

2.8. Statistical analysis

A two-way mixed analysis of variance (ANOVA) was used to analyze irrigation treatment effects (between-subject factor) over different time periods (within-subject factor) using rstatix package in R 4.1.0 (R Foundation for Statistical Computing, Vienna, Austria). Post hoc analysis was conducted to test differences between treatment means using the Bonferroni test. Data from all irrigation and cultivar treatments were used for 2018 and from all irrigation and PGR treatments for 2020 for the LAI, LWP_{PD}, and g_s analysis. A second-order polynomial regression was used to determine the relationship between all three CWSIs calculated and LWP_{PD}. The coefficient of determination (R^2) and the root mean square error (RMSE) were used to assess the CWSI ability to predict LWP_{PD}. The CWSI method with the highest R^2 and the lowest RMSE (MPa) was applied to the thermal images for LWP_{PD} prediction demonstration. The RMSE was calculated using Eq. 3.

$$RMSE = \sqrt{\frac{1}{n} x \sum_{i=1}^{n} (Pi - Oi)^2} \quad (3)$$

where n is the number of samples and Pi and Oi represent the predicted and observed values.

3. Results and discussion

3.1. Weather and Irrigation

Minimum and maximum air temperatures and precipitation during both growing seasons are represented in Fig. 4. Precipitation was high in 2018 with average monthly rainfall above 100 mm in May and June and above 200 mm towards the middle of the season, while in 2020, precipitation was lower at the beginning of the season and higher in August and September. Total water (rainfall + irrigation) per treatment in 2018 was more than 1.5 times the amount in 2020 due to the high precipitation (Table 1). Cotton grown in Georgia requires approximately 460 mm of water well distributed among the growth stages [9][41]. In 2018, precipitation was well above the cotton water requirement while in the second year, the precipitation was approximately 113 mm lower than that required.

Table 1
Irrigation, rainfall, and total water applied in both fields in Camilla, GA during the 2018 and 2020 growing seasons.

Year	Treatment	Irrigation	Precipitation	Total Water
		mm		
2018	Rainfed	0	828	828
	100% ET_c	220	828	1048
	125% ET_c	251	828	1079
2020	Rainfed	36	347	383
	100% ET_c	252	347	599
	125% ET_c	309	347	656

The approximate daily water requirement for cotton in humid regions from emergence to first square is around 2.54 mm [42][43]. This daily requirement ranges from 2.54 to 5.08 mm from first square to the first flower stage and reaches its peak between early flowering and peak bloom with daily water use increasing from 5.08 to 7.11 mm. Cotton plants are sensitive to water stress during squaring [42] and drought during this period can limit growth and number of nodes [44], but the highest sensitivity is seen during early bloom. Episodic drought in this period is critical and can lead to lower yield and lower fiber quality. After peak bloom, daily water use decreases, but cotton plants still have a moderate sensitivity to water stress. In 2018, precipitation was better distributed, and plants received enough water to supply their requirements in all growth stages. Contrary to 2018, in 2020 lower and inconsistent precipitation events caused episodic drought in the rainfed plots. Several consecutive days without rain caused the daily average precipitation to be 0.86 mm for the squaring period, which is well below cotton water needs for the same period. Similarly, in a period of 17 days during early bloom, total accumulated precipitation was only 7.87 mm.

3.2. Leaf area index (LAI)

LAI treatment averages are presented in Fig. 5. In both seasons, LAI overall trends were similar with low values during the initial stages of development, close to 1 at around 36 to 50 DAP, a rapid increase in canopy growth between 50 and 80 DAP, and a subsequent decrease at the end of the season. This peak curve response from early flowering to the open boll stage is often observed in cotton, independent of water regime [45]. During the 2018 season, excessive rainfall resulted in similar LAI values between the irrigation treatments and no significant differences were observed on any dates (Fig. 5a). Conversely, in 2020,

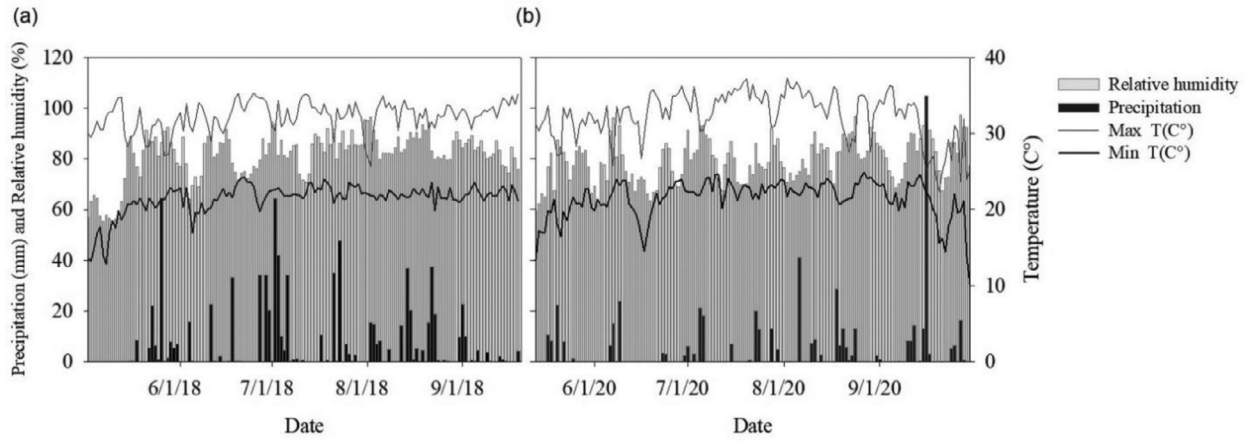

Fig. 4. Daily precipitation, relative humidity (%) and maximum and minimum air temperatures during the cotton growing season in 2018 (a) and 2020 (b).

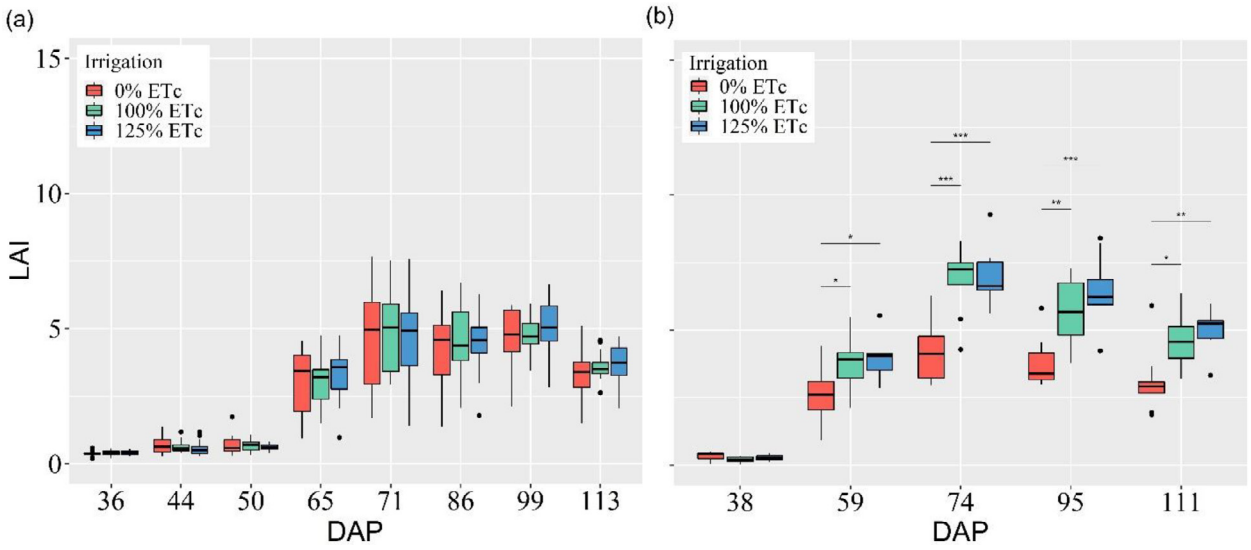

Fig. 5. Leaf area index (LAI) treatment averages and seasonal trends in Camila, GA in 2018 (a) and 2020 (b). The two-way mixed ANOVA results are represented in the figures as follow: $p<0.05$ (*), $p<0.01$(**), and $p<0.001$(***). Data represent means ± SE (2018; n = 18, 2020; n = 9).

rainfed and irrigated plots presented significant differences on all dates except 38 DAP (Fig. 5b). In the early season, irrigation was applied to all treatments to ensure stand establishment resulting in similar growth between treatments.

The highest treatment average LAI values in 2020 were achieved at 74 DAP with an average of 6.99, 6.79 and 4.26 for 125% ET_c, 100% ET_c and 0% ET_c treatments, respectively. Overall, the rainfed treatment had the lowest weekly averages with values being 38 to 45% lower than the well-watered treatment and 44 to 51% lower than the over-irrigated treatment. The greatest differences between treatments were seen at the peak flowering stage when maximum LAI was achieved. In contrast, when comparing irrigated treatments, well-watered and over-irrigated plots showed similar trends presenting no significant differences on any date. Similar irrigation regime effects on cotton LAI were observed by Noreen et al. [46]. The rainfed treatment had lower LAI with the greatest effects of drought being observed during the peak flowering stage in which plants achieved the highest LAI values and differences between treatments were more evident.

Leaf area is an important cotton morphological trait as it is a critical determinant of crop ET [47] and because of its influence on final yield [48]. Leaf area is very sensitive to drought once water stress leads to reduced cell division and expansion [49][50]. Noreen et al. [46] observed a high correlation between LAI and final total boll weight (r = 0.77) in well-watered conditions. This correlation was even more prominent when plants were exposed to drought conditions (r = 0.95) corroborating the assumption that the decrease in LAI due to water stress is a determinant factor of final yield.

3.3. Predawn Leaf water potential (LWP_{PD}) and stomatal conductance (g_s)

Seasonal weekly LWP_{PD} and g_s trends from both growing seasons are shown in Fig. 6. In 2018, significant differences in LWP_{PD} between irrigation treatments were observed in 6 out of the 8 dates evaluated (Fig. 6a). At 36 and 65 DAP, the 125% ET_c treatment had the highest LWP_{PD} values, while at all dates after 71 DAP the 0% ET_c (dryland) treatment had the highest values. Despite the differences between the irrigation treatments, measured LWP_{PD} remained relatively high during the whole season. The highest and lowest weekly LWP_{PD} averages observed for the whole season were -0.21 and -0.45 MPa, both from the 125% ET_c treatment. The low range in LWP_{PD} variability indicates that plants were not exposed to any water stress level which was a result of the high precipitation in that year. The absence of water stress is also reflected in the weekly treatment g_s averages (Fig. 6b). No significant differences in average g_s between the irrigation treatments were observed in 2018. The lowest and highest g_s values were observed for

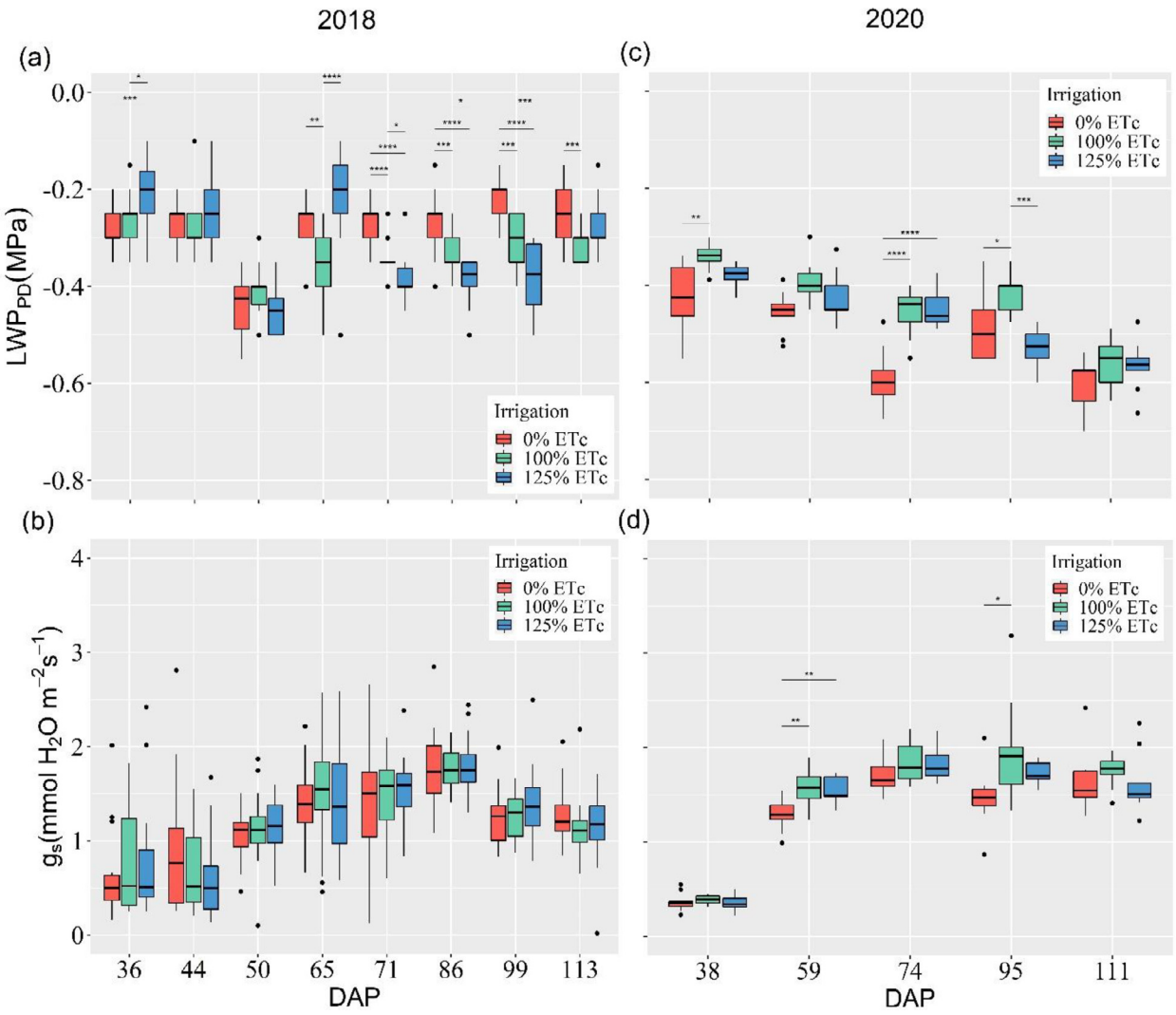

Fig. 6. Predawn leaf water potential (LWP_{PD}) expressed in MPa (a,c) and stomatal conductance (g_s) expressed in mmol H_2O $m^{-2}s^{-1}$ (b,d) treatment averages and seasonal trends for three difference irrigation treatments during the 2018 and 2020 growing seasons. The 2018 growing season is represented on the left panel and the 2020 in the right panel. The two-way mixed ANOVA results are represented in the figures as follow: p<0.05 (*), p<0.01(**), p<0.001(***), p<0.0001(****). Data represent means ± SE (2018; n = 18, 2020; n = 9).

the 125% ET_c treatment at 86 DAP (0.57 mmol H_2O $m^{-2}s^{-1}$) and at 44 DAP (1.79 mmol H_2O $m^{-2}s^{-1}$), respectively.

In the 2020 growing season, weekly irrigation treatment LWP_{PD} averages were significantly different on three separate occasions (Fig. 6c). Rainfed treatment averages significantly differed from the well-watered treatment at 38 DAP (p<0.001), 74 DAP (p<0.0001), and 95 DAP (p<0.05). The over-irrigated treatment was significantly different than rainfed at 74 DAP (p<0.0001), while well-watered and over-irrigated were significantly different at 95 DAP (p<0.001). The highest average LWP_{PD} value during the season was observed in the well-watered treatment (-0.34 MPa) followed by the over-irrigated treatment (-0.37 MPa). The lowest LWP_{PD} weekly average was observed for the rainfed (-0.6 MPa). The rainfed plots had an average LWP_{PD} value 16% lower than the 100% ET_c treatment. The decreased LWP_{PD} is a result of the isohydric response of cotton plants [51][1] in which the water potential in the leaf decreases in response to a lower soil water potential.

As previously shown, canopy growth was substantially reduced in the rainfed plots displaying a lower LAI than irrigated treatments in 2020. Chastain et al. [22] pointed out that plant growth inhibition was only observed when LWP_{PD} reached values below -0.8 MPa. Although measured LWP_{PD} values for the second season were higher than that threshold, a more severe drought occurred during the season in the weeks in-between measurements. Despite these periods of low precipitation not coinciding with LWP_{PD} field sampling days, the drought effects were prominent in the rainfed plots and can be detected by the leaf area differences between rainfed and irrigated treatments.

Stomatal conductance (g_s) treatment averages were statistically different on two separate occasions for the 2020 growing season (Fig. 6d). The rainfed treatment g_s average was significantly lower than the well-watered and the over-irrigated treatments (p<0.0001) at 59 DAP, and lower than the well-watered treatment (p<0.05) at 95 DAP, while both irrigated treatments showed significant differences (p<0.001) only at 95 DAP. Similar to the results seen for LWP_{PD}, g_s average values were frequently lower in the rainfed plots. Well-watered and over-irrigated treatments had similar average g_s throughout the season and did not show any significant difference.

The reduction in leaf stomatal conductance is a mechanism commonly seen in drought stressed plants to limit water loss [52]. A lower leaf water potential is observed when soil water availability is decreased, which triggers stomatal closure [53]. In the same study, a substantial decrease in g_s was detected three days after plants were exposed to drought. A recent study indicated that g_s in rainfed plots was 72 and 58% lower than irrigated treatments in two consecutive years [1]. Pi-

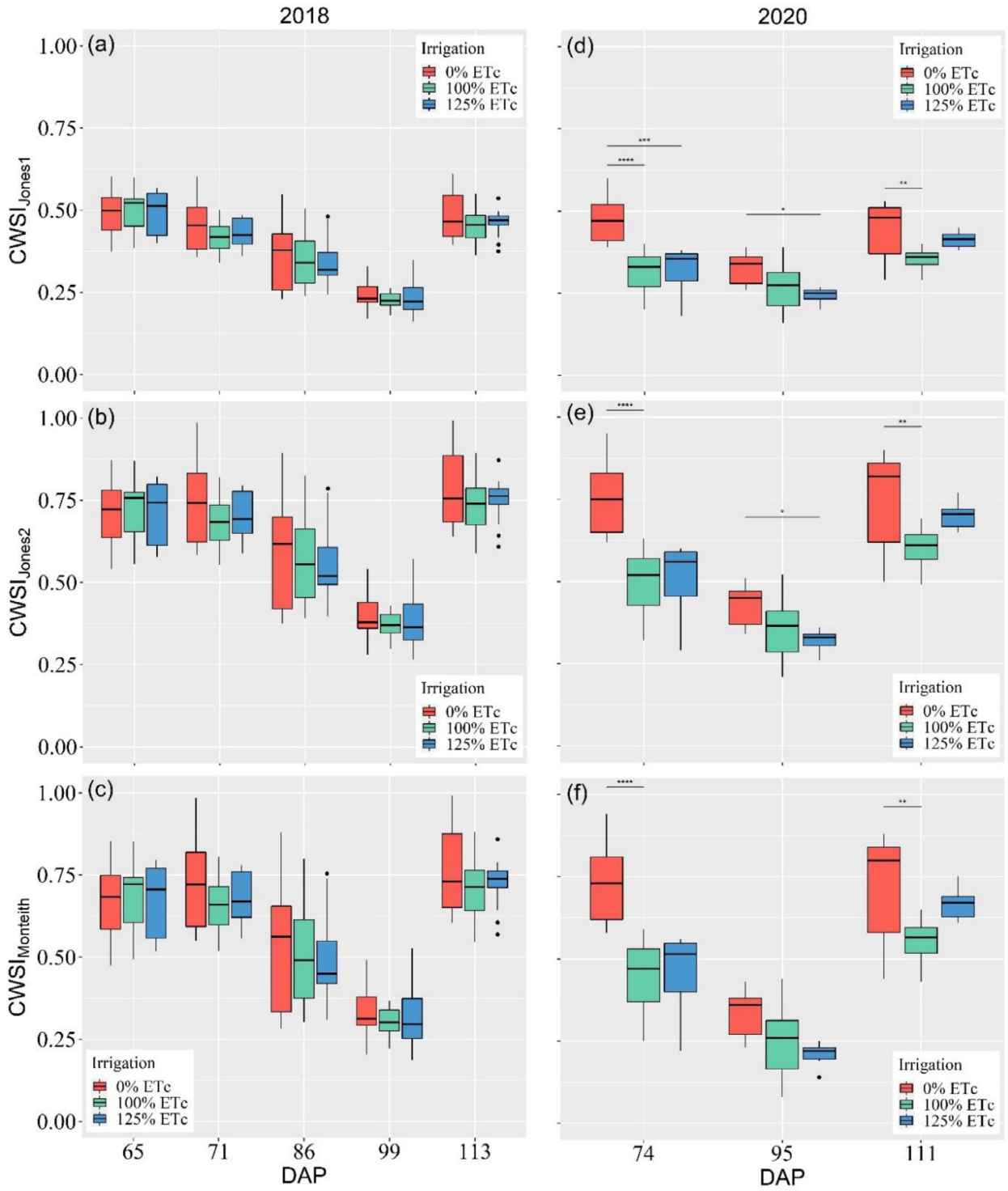

Fig. 7. Crop water stress index (CWSI) approaches treatment averages and seasonal trends for three difference irrigation treatments during the 2018 and 2020 growing seasons. The 2018 growing season is represented on the left panel and the 2020 in the right panel. The two-way mixed ANOVA results are represented in the figures as follow: $p<0.05$ (*), $p<0.01$(**), $p<0.001$(***), $p<0.0001$(****). Data represent means ± SE (2018; n = 18, 2020; n = 9).

lon et al. [53] observed even higher differences of 81% between well-watered and drought stressed cotton plants.

3.4. Crop water stress index (CWSI)

Fig. 7 shows the weekly treatment CWSI values calculated using the three different methodologies. All methods yielded similar seasonal trends in both years. In 2018, no significant differences were seen between the treatment CWSI averages in any of the dates observed (Fig. 7a-c). The 100% ET_c treatment had the lowest CWSI values observed during the season varying from 0.23, 0.3 and 0.37 for $CWSI_{jones1}$, $CWSI_{Monteith}$ and $CWSI_{Jones2}$, respectively. The highest stress level calculated using $CWSI_{Jones1}$ methodology was 0.5 and it was observed for the 100% ET_c treatment at 65 DAP, while for $CWSI_{Monteith}$, $CWSI_{Jones2}$ the highest stress indices were seen for the 0% ET_c treatment at 113 DAP (0.78 and 0.76, respectively).

Table 2
Regression models between CWSI and LWP_{PD} on different dates in 2018 and 2020.

Year	DAP	CWSI method	Equation	R^2	RMSE (MPa)
2018	**65**	Jones 1	$y = -0.198x^2 - 0.302x - 0.124$	0.37	0.05
		Jones 2	$y = -0.268x^2 - 0.018x - 0.175$	0.38	0.05
		Monteith	$y = -0.222x^2 - 0.057x - 0.186$	0.38	0.05
	71	Jones 1	$y = 2.388x^2 - 1.761x - 0.163$	0.47	0.04
		Jones 2	$y = 0.729x^2 - 0.308x - 0.565$	0.43	0.04
		Monteith	$y = 0.544x^2 - 0.091x - 0.598$	0.43	0.04
	86	Jones 1	$y = -9.999x^2 + 6.294x - 1.301$	0.35	0.04
		Jones 2	$y = -6.218x^2 + 4.879x - 1.268$	0.34	0.04
		Monteith	$y = -4.020x^2 + 2.004x - 0.560$	0.33	0.04
	99	Jones 1	$y = -7.202x^2 + 5.726x - 1.425$	0.09	0.06
		Jones 2	$y = -5.637x^2 + 4.549x - 1.205$	0.08	0.06
		Monteith	$y = -3.398x^2 + 1.722x - 0.506$	0.08	0.06
	113	Jones 1	$y = 9.132x^2 - 8.461x + 1.672$	0.15	0.03
		Jones 2	$y = 2.004x^2 - 2.843x + 0.723$	0.04	0.03
		Monteith	$y = 3.138x^2 - 4.177x + 1.102$	0.15	0.03
2020	**74**	Jones 1	$y = 0.348x^2 - 0.789x - 0.258$	0.57	0.04
		Jones 2	$y = 0.144x^2 - 0.504x - 0.256$	0.57	0.04
		Monteith	$y = 0.105x^2 - 0.420x - 0.304$	0.58	0.04
	95	Jones 1	$y = 9.483x^2 - 4.832x + 0.101$	0.46	0.04
		Jones 2	$y = 5.136x^2 - 3.410x + 0.052$	0.44	0.04
		Monteith	$y = 3.795x^2 - 1.672x - 0.330$	0.45	0.04
	111	Jones 1	$y = -7.5207x^2 + 5.9x - 1.7061$	0.65	0.02
		Jones 2	$y = -2.6216x^2 + 3.4957x - 1.7137$	0.65	0.02
		Monteith	$y = -2.1493x^2 + 2.6977x - 1.3949$	0.65	0.02

In 2020, CWSI treatment average values were significantly different on all dates for the Jones 1 and Jones 2 approaches and on two dates (74 and 111 DAP) using the Monteith equation (Fig. 7d-f). Rainfed plots showed significantly higher CWSI values than the 100% ET_c treatment for all CWSIs calculated at 74 DAP ($p<0.0001$) and at 111 DAP ($p<0.01$). Rainfed and the 125%ET_c treatments were significantly different for Jones 1 and Jones 2 approaches at 95 DAP ($p<0.05$) and only for Jones 1 at 74 DAP ($p<0.001$). Overall, in both seasons $CWSI_{Jones1}$ using theoretical dry and wet baselines tended to yield lower values than Jones 2 and Monteith approaches using an empirical dry baseline. These differences can be attributed to the limitations of the energy balance model used in the theoretical approach. Energy balance models rely on the characteristics of a virtual leaf that represents the average leaf parameters, and it assumes that the leaf is in equilibrium with its surroundings [28]. Any variations from these parameters can cause inaccuracies that can lead to the dry baseline being higher or lower than empirically calculated baselines.

3.5. Simple regression models for cotton LWP_{PD} prediction

The $CWSI/LWP_{PD}$ models were developed for all three CWSI methodologies in 5 different dates in 2018 and 3 dates in 2020. Table 2 presents equations, and performance for all models developed. Performance was evaluated based on R^2 and RMSE.

In 2018, prediction models showed a weak to moderate relationship between CWSI and LWP_{PD} likely due to the low variability in water status among the plots. The strongest relationships were observed at 71 DAP with R^2 of 0.47, 0.43 and 0.43 for $CWSI_{Jones1}$, $CWSI_{Jones2}$ and $CWSI_{Monteith,}$ respectively, followed by the models at 65 DAP with an average R^2 value of 0.38 and at 86 DAP with average R^2 of 0.34. Lowest R^2 values were observed at 99 DAP ranging from 0.08 for $CWSI_{Jones2}$ and $CWSI_{Monteith}$ to 0.09 for $CWSI_{Jones1}$. The highest RMSE values were also observed at 99 DAP with values of 0.06 MPa for all 3 approaches. Overall, prediction errors were relatively low with values varying from 0.03 to 0.06 for all dates. The best performing model in all dates was developed based on $CWSI_{Jones1,}$ which showed a slightly higher R^2 except for 65 DAP, in which $CWSI_{Jones2}$ and $CWSI_{Monteith}$ had slightly higher R^2.

In 2020, all CWSIs had a moderate to strong non-linear relationship with LWP_{PD}. Best performing models were observed at 111 DAP with a R^2 of 0.65 and an RMSE of 0.02 MPa for all three CWSIs. Prediction models at 74 DAP had R^2 values of 0.57 for both $CWSI_{Jones1}$ and $CWSI_{Jones2}$ and of 0.58 for $CWSI_{Monteith}$, and an error of 0.04 MPa. Model performances were lower at 95 DAP with R^2 values of 0.46, 0.44 and 0.45 for $CWSI_{Jones1}$, $CWSI_{Jones2}$ and $CWSI_{Monteith,}$ respectively, and RMSE of 0.04 for all three methods. Models performed very similarly in the second season. $CWSI_{Jones1}$ had a slightly higher R^2 at 74 DAP, and $CWSI_{Monteith}$ was slightly higher at 95 DAP.

The relationship between CWSI and LWP_{PD} for the southeastern US was originally developed by Chastain et al. [22] in a study conducted during 2016 in the same region as the present study but using in-field infrared proximal canopy temperature sensors. A non-linear relationship between CWSI and LWP_{PD} was also observed with a coefficient of determination of 0.93. Results from the 2016 study showed a wider variation in LWP_{PD}. In contrast to the Chastain et al. study, the CWSIs in the work reported here were calculated from UAV-based sensors with temperature measured over plot-sized areas and still showed moderate to relatively strong relationships on selected dates despite the lower variation in LWP_{PD}. Calculated CWSI values for plots with higher LWP_{PD} were overall higher than observed by Chastain et al. [22] indicating an overestimation of the canopy temperature measured from the UAV camera when compared to proximal infrared sensors.

Results from the present work using empirical, and theoretical baselines and from Chastain et al. [22] using empirical wet and dry baselines from Idso [38] indicated a non-linear relationship between CWSI and LWP in the humid southeast of the U.S.A. Alchanatis et al. [28] developed the CWSI/LWP relationship for cotton using empirical and theoretical baselines and found a strong linear relationship. The work was

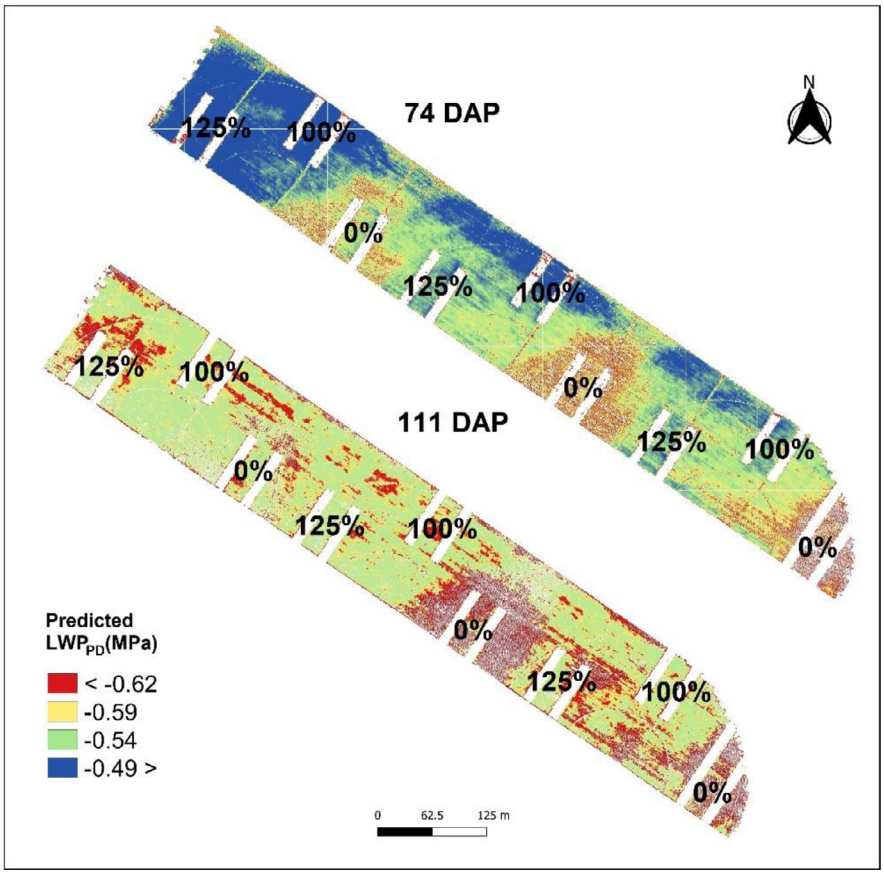

Fig. 8. Predicted LWP_{PD} maps based on the $CWSI_{Monteith}$ models developed at 74 DAP and 111 DAP in 2020.

conducted in Israel where there is a Mediterranean climate with low humidity during the growing season. A similar linear relationship was also observed in the arid environment of northwestern Texas, U.S.A. using empirical CWSI [54]. These results suggest that the relationship between different CWSI and LWP_{PD} is region-specific and should be developed taking different environmental conditions into account.

Weekly models with R^2 higher than 0.5 were used to create predicted LWP_{PD} maps. The model derived from the $CWSI_{Monteith}$ was selected for application as this model had the highest R^2 among the different approaches at 74 DAP. The $CWSI_{Monteith}/LWP_{PD}$ equations were applied to the UAV images at 74 and 111 DAP to produce the two predicted LWP_{PD} maps shown on Fig. 8.

The maps indicate that the variability in LWP_{PD} seen in this study was not only a function of the irrigation treatments but also the spatial variability of the soils and their water holding capacity in the study field. Cohen et al. [55] highlighted the usefulness of using the CWSI/LWP relationship to create estimated LWP maps throughout the season. The ability to monitor plant water status from canopy temperature can help improve irrigation management decisions based on crop water needs even in the southeastern U.S. where humidity and frequent cloud cover makes this methodology challenging [19]. This statement is corroborated by the results from this study. The different water status patterns resulting from the irrigation treatments can be easily identified in the field. In both dates, irrigated treatments showed higher predicted LWP_{PD} when compared to rainfed. The different patterns are more prominent at 74 DAP in which color classification varies from blue to red representing the lowest to highest LWP_{PD} values, respectively.

4. Conclusions

Results from this study suggest that LWP_{PD} values above -0.45 MPa indicate a non-stressed crop and no negative effects in leaf stomatal conductance or crop growth were observed as represented in the 2018 growing season. In 2020, the lower and more irregular precipitation events led to significant differences in LAI and g_s, as well as in LWP_{PD}. Irrigated treatments (well-irrigated, and over-irrigated) tended to show higher LWP_{PD}, LAI and g_s than rainfed treatments, indicating that growth limitation occurred in the non-irrigated plots due to drought stress. Field measurement dates did not coincide with peak stress periods. Although the lowest average LWP_{PD} value recorded during the season was -0.6 MPa, rainfed plots experienced an extended drought period for about 17 days during flowering. Despite the somewhat high LWP_{PD} values, the different CWSIs showed a moderate to relatively strong non-linear relationship with LWP_{PD}, indicating that UAV-based thermal data has the potential to detect water status patterns even in less severe drought periods.

CWSI methodologies yielded similar results in the 8 dates analyzed in both years. Despite the overall lower values obtained from the $CWSI_{Jones1}$ calculated with theoretical wet and dry baselines, the relationship between all CWSIs and LWP_{PD} had similar R^2 and RMSE. Best performing models were observed in 2020 with moderate to relatively strong relationships in all dates in 2020, with the $CWSI_{Monteith}$ showing the two highest R^2 values among the 3 dates (0.65 and 0.58) with low RMSE values of 0.02 and 0.04 MPa, respectively.

Overall, the results showed potential of using an affordable UAV-thermal system to produce predicted LWP maps that are representative of the current field water status in the humid southeastern U.S.A. The utilization of these maps can enable farmers to monitor crop water status variability across the field during the season and help improve irrigation management decisions. Moreover, these maps can be potentially used to develop dynamic variable rate irrigation systems through the delineation of crop-based in-season irrigation management zones.

Declaration of interests

The authors declare that they have no known competing financial interests or personal relationships that could have appeared to influence the work reported in this paper.

Acknowledgment

This project was funded by US-Israel Binational Agricultural Research and Development Fund (BARD) Research Project US-4991-1 and by Georgia Agricultural Commodity Commission for Cotton Project No. 12-173GA-7. Special thanks to the University of Georgia's Stripling Irrigation Research Park and its staff for hosting and supporting the study.

References

[1] D.R. Chastain, J.L. Snider, G.D. Collins, C.D. Perry, J. Whitaker, S.A. Byrd, Water deficit in field-grown *Gossypium hirsutum* primarily limits net photosynthesis by decreasing stomatal conductance, increasing photorespiration, and increasing the ratio of dark respiration to gross photosynthesis, J. Plant Physiol. 171 (2014) 1576–1585, doi:10.1016/j.jplph.2014.07.014.

[2] USDA. NASS- United Stated Department of Agriculture National Agricultural Statistics Service. https://www.nass.usda.gov/Statistics_by_Subject/, 2021 (accessed on 09 September 2021).

[3] T. Feike, L.Y. Khor, Y. Mamitimin, N. Ha, L. Li, N. Abdusalih, H. Xiao, R. Doluschitz, Determinants of cotton farmers' irrigation water management in arid Northwestern China, Agric. Water Manag. 187 (2017) 1–10, doi:10.1016/j.agwat.2017.03.012.

[4] O. Cetin, S. Basbag, Effects of climatic factors on cotton production in semi-arid regions - A review, Res. on Crops 11 (3) (2010) 785–791.

[5] G.A. Constable, M.P. Bange, The yield potential of cotton (*Gossypium hirsutum* L.), Field Crops Res 182 (2015) 98–106, doi:10.1016/j.fcr.2015.07.017.

[6] A.B. Hearn, Water relationships in cotton, Outlook Agric 10 (4) (1980) 159–166, doi:10.1177/003072708001000402.

[7] N.C. Turner, A.B. Hearn, J.E. Begg, G.A. Constable, Cotton (*Gossypium Hirsutum L.*): Physiological and morphological responses to water deficits and their relationship to yield, Field Crops Res 14 (1986) 153–170, doi:10.1016/0378-4290(86)90054-7.

[8] NOAA- National Oceanic and Atmospheric Administration (2021) https://www.ncdc.noaa.gov/climate-monitoring/. (accessed on 09 July 2021).

[9] C. Bednarz, G. Ritchie, J. Hook, R. Yager, S. Cromer, D. Cook, I. Griner, Cotton crop water use and irrigation scheduling, in: A.S. Culpepper (Ed.), Georgia Cotton Research-Extension Report, Univ. of Georgia, Athens, GA, USA, 2002, pp. 61–64.

[10] R. Wang, P. Zhang, Y. Meng, Y. Wang, B. Chen, Z. Zhou, Drought effect on cotton yield and fiber quality on different fruiting branches, Crop Sci 56 (2016) 1265–1276, doi:10.2135/cropsci2015.08.0477.

[11] W. Hu, J.L. Snider, H. Wang, Z. Zhou, D.R. Chastain, J. Whitaker, C.D. Perry, F.M. Bourland, Water-induced variation in yield and quality can be explained by altered yield component contributions in field-grown cotton, Field Crops Res 224 (2018) 139–147, doi:10.1016/j.fcr.2018.05.013.

[12] D.A. Loka, D.M. Oosterhuis, G.L. Ritchie, Water-Deficit Stress in Cotton, in: D.M. Oosterhuis (Ed.), Stress Physiology in Cotton, The Cotton Foundation, Memphis, Tenn., 2011, pp. 37–72.

[13] A. Yazar, S.M. Sezen, S. Sesveren, LEPA and trickle irrigation of cotton in the Southeast Anatolia Project (GAP) area in Turkey, Agric. Water Manag. 54 (3) (2002) 189–203, doi:10.1016/S0378-3774(01)00179-2.

[14] J. Soth, C. Grasser, R. Salerno, The impact of cotton on freshwater resources and ecosystems: A preliminary synthesis, Worldwide Fund for Nature, WWF, Gland, Switzerland, 1999.

[15] G. Vellidis, V. Liakos, J.H. Andreis, C.D. Perry, W.M. Porter, E.M. Barnes, K.T. Morgan, C. Fraisse, K.W. Migliaccio, Development and assessment of a smartphone application for irrigation scheduling in cotton, Comput. Electron. Agric. 127 (2016) 249–259, doi:10.1016/j.compag.2016.06.021.

[16] G. Vellidis, V. Liakos, W. Porter, M. Tucker, X. Liang, A dynamic variable rate irrigation control system, in: 13th International Conference on Precision Agriculture, St. Louis, Missouri, 2016.

[17] C.D. Meeks, J.L. Snider, W.M. Porter, G. Vellidis, G. Hawkins, D. Rowland, Assessing the utility of primed acclimation for improving water savings in cotton using a sensor-based irrigation scheduling system, Crop Sci 57 (4) (2017) 2117–2129, doi:10.2135/cropsci2016.10.0907.

[18] F. Li, Y. Dong, Y. Zhao, Irrigation scheduling optimization for cotton based on the AquaCrop model, Water Resour. Manag. 33 (2019) 39–55, doi:10.1007/s11269-018-2087-1.

[19] H.G. Jones, Irrigation scheduling: advantages and pitfalls of plant-based methods, J. Exp. Bot. 55 (2004) 2427–2436, doi:10.1093/jxb/erh213.

[20] D.W. Grimes, H. Yamada, Relation of cotton growth and yield to minimum leaf water potential, Crop Sci 22 (1) (1982) 134–139, doi:10.2135/cropsci1982.0011183X002200010031x.

[21] D.W. Grimes, H. Yamada, S.W. Hughes, Climate-normalized cotton leaf water potentials for irrigation scheduling, Agric. Water Manag. 12 (4) (1987) 293–304, doi:10.1016/0378-3774(87)90004-7.

[22] D.R. Chastain, J.L. Snider, G.D. Collins, C.D. Perry, J. Whitaker, S.A. Byrd, D.M. Oosterhuis, W.M. Porter, Irrigation Scheduling using predawn leaf water potential improves water productivity in drip-irrigated cotton, Crop Sci 56 (6) (2016) 3185–3195, doi:10.2135/cropsci2016.01.0009.

[23] J. Bellvert, P.J. Zarco-Tejada, J. Marsal, J. Girona, V. Gonzalez-Dugo, E. Fereres, Vineyard irrigation scheduling based on airborne thermal imagery and water potential thresholds, Aust. J. Grape Wine Res. 22 (2) (2016) 307–315, doi:10.1111/ajgw.12173.

[24] T.A. Paço, M.I. Ferreira, C.A. Pacheco, Scheduling peach orchard irrigation in water stress conditions: use of relative transpiration and predawn leaf water potential, Fruits 68 (2) (2013) 147–158, doi:10.1051/fruits/2013061.

[25] I.G. Argyrokastritis, P.T. Papastylianou, S. Alexandris, Leaf water potential and crop water stress index variation for full and deficit irrigated cotton in Mediterranean conditions, Agric. Agric. Sci. Procedia 4 (2015) 463–470, doi:10.1016/j.aaspro.2015.03.054.

[26] R.D. Jackson, Canopy temperature and crop water stress, Adv. Irrig. 1 (1982) 43–85, doi:10.1016/B978-0-12-024301-3.50009-5.

[27] S. Elsayed, B. Mistele, U. Schmidhalter, Can changes in leaf water potential be assessed spectrally? Funct. Plant Biol. 38 (2011) 523–533, doi:10.1071/FP11021.

[28] V. Alchanatis, Y. Cohen, S. Cohen, M. Moller, M. Sprinstin, M. Meron, J. Tsipris, Y. Saranga, E. Sela, Evaluation of different approaches for estimating and mapping crop water status in cotton with thermal imaging, Precision Agric 11 (2010) 27–41, doi:10.1007/s11119-009-9111-7.

[29] O. Rosenberg, V. Alchanatis, Y. Cohen, Are thermal images adequate for irrigation management?, in: J.V. Stafford (Ed.) The 12th International conference on precision agriculture, Sacramento, CA, 2014.

[30] Y. Cohen, V. Alchanatis, M. Meron, Y. Saranga, J. Tsipris, Estimation of leaf water potential by thermal imagery and spatial analysis, J. Exp. Bot. 56 (417) (2005) 1843–1852, doi:10.1093/jxb/eri174.

[31] Y. Cohen, V. Alchanatis, E. Sela, Y. Saranga, S. Cohen, M. Meron, A. Bosak, V. Tsipris, V. Ostrovsky, V. Orolov, A. Levi, R. Brikman, Crop water status estimation using thermography: multi-year model development using ground-based thermal images, Precision Agric.16 (2015) 311-329. https://doi.org/10.1007/s11119-014-9378-1

[32] S.J. Thomson, C.M. Ouellet-Plamondon, S.L. DeFauw, Y. Huang, D.K. Fisher, P.J English, Potential and challenges in use of thermal imaging for humid region irrigation system management, J. Agric. Sci. 4 (4) (2012), doi:10.5539/jas.v4n4p103.

[33] G. Bodner, A. Nakhforoosh, H.P. Kaul, Management of crop water under drought: a review, Agron. Sustain. Dev. 35 (2015) 401–442, doi:10.1007/s13593-015-0283-4.

[34] H.G. Jones, R. Serraj, B.R. Loveys, L. Xiong, A. Wheaton, A.H. Price, Thermal infrared imaging of crop canopies for the remote diagnosis and quantification of plant responses to water stress in the field, Funct. Plant Biol. 36 (2009) 978–989, doi:10.1071/FP09123.

[35] D.A. Pennington, L. Heatherly, Effects of changing solar radiation on canopy-air temperatures of cotton and soybeans, Agric. For. Meteorol. 46 (1989) 1–14, doi:10.1016/0168-1923(89)90108-1.

[36] M. Meron, J. Tsipris, V. Orlov, V. Alchanatis, Y. Cohen, Crop water stress mapping for site-specific irrigation by thermal imagery and artificial reference surfaces, Precision Agric.11 (2010) 148-162. https://doi.org/10.1007/s11119-009-9153-x

[37] M. Gerhards, G. Rock, M. Schlerf, T. Udelhoven, Water stress detection in potato plants using leaf temperature, emissivity, and reflectance, Int. J. Appl. Earth Obs. and Geoinf. 53 (2016) 27–39, doi:10.1016/j.jag.2016.08.004.

[38] S.B. Idso, R.D. Jackson, J.J. Pinter Jr., R.J. Reginato, J.L. Hatfield, Normalizing the stress-degree-day parameter for environmental variability, Agric. Meteorol. 24 (1981) 45–55, doi:10.1016/0002-1571(81)90032-7.

[39] H.G. Jones, Use of infrared thermometry for estimation of stomatal conductance as a possible aid to irrigation scheduling, Agric. For. Meteorol. 95 (3) (1999) 139–149, doi:10.1016/S0168-1923(99)00030-1.

[40] J.L. Monteith, M.L. Unsworth, Principles of environmental physics, Edward Arnold, London, UK, 1990.

[41] G.L. Ritchie, J.R. Whitaker, C.W. Bednarz, J.E. Hook, Subsurface drip and overhead irrigation: a comparison of plant boll distribution in upland cotton, Agron. J. 101 (6) (2009) 1336–1344, doi:10.2134/agronj2009.0075.

[42] P. Bauer, W. Faircloth, D. Rowland, G. Richie, Water sensitivity of cotton growth stages, in: C. Perry, E. Barnes (Eds.), Cotton Irrigation Management for Humid Regions, Cotton Incorporated, 2012.

[43] D.K. Fisher, Simple and inexpensive lysimeters for monitoring reference- and crop-ET, in: Proceedings of the 25th Annual International Irrigation Conference, November 14-16, Tampa, Florida, 2004.

[44] M.C. Snowden, G.L. Ritchie, F.R. Simao, J.P. Bordovsky, Timing of episodic drought can be critical in cotton, Crop Ecol. Physiol. 106 (2) (2014) 452–458, doi:10.2134/agronj2013.0325.

[45] D. Zhang, Z. Luo, S. Liu, W. Li, Wei Tang, H. Dong, Effects of deficit irrigation and plant density on the growth, yield and fiber quality of irrigated cotton, Field Crops Res 197 (2016) 1–9, doi:10.1016/j.fcr.2016.06.003.

[46] S. Noreen, H.U.R. Athar, M. Ashraf, Interactive effects of watering regimes and exogenously applied osmoprotectants on earliness indices and leaf area index in cotton (*Gossypium hirsutum* L.) crop, Pak. J. Bot. 45 (2013) 1873–1881.

[47] S. Al-Khafaf, P.J. Wierenga, B.C. Williams, Evaporative flux from irrigated cotton as related to leaf area index, soil water, and evaporative demand, Agron. J. 70 (1978) 912–917.

[48] M.F. Saleem, M.A.S. Raza, S. Ahmad, I.H. Khan, A.M. Shahid, Understanding and mitigating the impacts of drought stress in cotton- a review, Pak. J. Bot. 53 (3) (2016) 609–623.

[49] A.A.C. Alves, T.L. Setter, Response of cassava leaf area expansion to water deficit: cell proliferation, cell expansion and delayed development, Ann. Bot. 94 (4) (2004) 605–613, doi:10.1093/aob/mch179.

[50] G. Koch, G. Rolland, M. Dauzat, A. Bédiée, V. Baldazzi, N. Bertin, Y. Guedon, C. Granier, Leaf production and expansion: A generalized response to drought stresses from cells to whole leaf biomass- A case study in the tomato compound leaf, Plants 8 (10) (2019) 409, doi:10.3390/plants8100409.

[51] F. Tardieu, T. Simonneau, Variability among species of stomatal control under fluctuating soil water status and evaporative demand: modeling isohydric and anisohydric behaviors, J. Exp. Bot. 49 (1998) 419–432, doi:10.1093/jxb/49.Special_Issue.419.

[52] X. Li, R. Smith, B. Choat, D.T. Tissue, Drought resistance of cotton (*Gossypium hirsutum*) is promoted by early stomatal closure and leaf shedding, Funct. Plant Biol. 47 (2) (2020) 91–98, doi:10.1071/FP19093.

[53] C. Pilon, D. Loka, J.L. Snider, D.M. Oosterhuis, Drought-induced osmotic adjustment and changes in carbohydrate distribution in leaves and flowers of cotton (*Gossypium hirsutum* L.), J. Agron. Crop Sci. 205 (2) (2018) 168–178, doi:10.1111/jac.12315.

[54] S.A. O'Shaughnessy, S.R. Evett, P.D. Colaizzi, T.A. Howell, Using radiation thermography and thermometry to evaluate crop water stress in soybean and cotton, Agric. Water Manag. 98 (10) (2011) 1523–1535, doi:10.1016/j.agwat.2011.05.005.

[55] Y. Cohen, V. Alchanatis, Y. Saranga, O. Rosenberg, E. Sela, A. Bosak, Mapping water status based on aerial thermal imagery: comparison of methodologies for upscaling from a single leaf to commercial fields, Precision Agric. 18 (2017) 801-822. doi:10.1007/s11119-016-9484-3.